Band Structure and Fermi Surface of Gallium by the Pseudopotential Method

W. A. REED
Bell Telephone Laboratories, Murray Hill, New Jersey 07974
(Received 16 June 1969)

The band structure of gallium has been calculated using a local semiempirical pseudopotential without spin-orbit coupling. The Fermi surface consists of six closed electron sheets, one closed hole sheet, and a large multiply-connected hole sheet. The calculated surface explains much of the experimental data and is a good representation of the larger pieces. However, the analysis of the data indicates that one or more very small pieces may have been missed in the calculation. Condon's unpublished de Haas–van Alphen data are included in the Appendix.

I. INTRODUCTION

ALTHOUGH extremely pure single crystals of gallium[1] are easily prepared and Fermi-surface data from a variety of experimental techniques[2] are readily obtained, the complexity of the data has prohibited all but an initial interpretation in terms of a Fermi-surface model. Likewise, calculations using the one-orthogonalized-plane-wave (1-OPW)[3,4] or augmented-plane-wave (APW)[5] methods have been unable to produce band structures capable of interpreting most aspects of the experimental data.

In this paper, the results of a local semiempirical pseudopotential calculation without spin-orbit effects are presented. The primary goal of this calculation is to determine the number of Fermi-surface pieces together with their approximate sizes and shapes. The quantitative agreement between the calculation and experiment, although reasonably good, is not stressed and parts of the calculated surface are adjusted in order to relate them to the data. All of the Fermi-surface pieces which appear in the calculation can be found in the data, but the data also suggest that one or more very small pieces may have been missed. It is hoped that this first approximation will encourage more detailed and precise data, and this in turn will lead to more elegant calculations.

For gallium, the pseudopotential method of calculating band structures is more appropriate than either the 1-OPW method or the APW method using the muffin-tin potential. As Wood[5] pointed out, a large number of accidental degeneracies occur in the 1-OPW model as a result of the low crystal symmetry. Since, in fact, most of these degeneracies are removed by the lattice potential, it is reasonable to expect that the true Fermi surface is not similar to the nearly-free-electron Fermi surface. Likewise, it is not surprising that the APW calculation has not been particularly successful in explaining the Fermi-surface data, since the muffin-tin potential[5] approximates 60% of the total cell volume with a constant potential, leaving only 40% of the volume inside the APW spheres. Since the pseudopotential method is expected to do a better job of approximating the true potential throughout the cell, it should be more successful than the other two methods.

The pseudopotential form factor used in this calculation is based on the Animalu-Heine[6] model potential for gallium and the Cohen-Bergstresser[7] potentials for GaAs, GaP, and GaSb. It is represented by a simple analytical expression involving five parameters which were empirically adjusted to give the best agreement between the calculated Fermi surface and the data. This semiempirical form factor differs slightly but significantly from the form factors used by Inglesfield[8] in his calculation of the gallium structure and phase changes, and from the form factor for a model potential calculated by Ashcroft.[9]

[1] Electron mean free paths of 1 cm at 1.5°K have been reported by B. W. Roberts, Phys. Rev. Letters **6**, 453 (1961).

[2] de Haas–van Alphen effect: A. Goldstein and S. Foner, Phys. Rev. **146**, 442 (1966); J. H. Condon, Bull. Am. Phys. Soc. **9**, 239 (1964); see Appendix of the present paper for Condon's data. rf size effect: D. M. Sparlin and D. S. Shrieber, in *Proceedings of the Ninth International Conference on Low Temperature Physics, Columbus, Ohio, 1964*, edited by J. G. Daunt, D. O. Edwards, F. J. Milford, and M. Yaqub (Plenum Press, Inc., New York, 1965), part B, p. 823; A. Fukumoto and M. W. P. Strandberg, Phys. Rev. **155**, 685 (1967); P. H. Haberland, J. F. Cochran, and C. A. Shiffman, *ibid.* **189**, 000 (1969). Magnetoacoustic attenuation: Ref. 1 and P. A. Bezuglyi, A. A. Galkin, and S. E. Zhevago, Zh. Eksperim. i Teor. Fiz. **47**, 825 (1964) [English transl.: Soviet Phys.—JETP **20**, 552 (1965)]; P. A. Bezuglyi, A. A. Galkin, and S. E. Zhevago, Fiz. Tverd. Tela **7**, 480 (1965) [English transl.: Soviet Phys.—Solid State **7**, 383 (1965)]; J. Lewiner, Comp. Rend. **265B**, 774 (1967). Galvanomagnetic effects: W. A. Reed and J. A. Marcus, Phys. Rev. **126**, 1298 (1962); J. R. Cook and W. R. Datars, in *Proceedings of the Eleventh International Conference on Low Temperature Physics, St. Andrews, Scotland, 1968*, edited by J. F. Allen, D. M. Finlayson, and D. M. McCall (University of St. Andrews Printing Dept., Scotland, 1969), p. 1137; and (private communication); J. C. Kimball and R. W. Stark (unpublished). Cyclotron resonance: J. Lewiner, Phys. Rev. Letters **19**, 1037 (1967); T. W. Moore, Phys. Rev. **165**, 864 (1968); J. A. Munarin, *ibid.* **172**, 737 (1968). Size-dependent oscillatory magnetoresistance: J. A. Munarin, J. A. Marcus, and P. E. Bloomfield, *ibid.* **172**, 718 (1968). Magnetothermal effect: P. Goy, A. Goldstein, D. N. Langenberg, and J. C. Picard, Phys. Letters **25A**, 324 (1967). Oscillatory magnetostriction: P. A. Penz, Bull. Am. Phys. Soc. **14**, 29 (1969).

[3] W. A. Reed and J. A. Marcus, Ref. 2.

[4] J. C. Slater, G. F. Koster, and J. H. Wood, Phys. Rev. **126**, 1307 (1962).

[5] J. H. Wood, Phys. Rev. **146**, 432 (1966).

[6] A. O. E. Animalu and V. Heine, Phil. Mag. **12**, 1249 (1965). The potential is tabulated in Ref. 10, p. 309.

[7] M. L. Cohen and T. K. Bergstresser, Phys. Rev. **141**, 789 (1966).

[8] J. E. Inglesfield, J. Phys. **C1**, 1337 (1968).

[9] N. W. Ashcroft (private communication). Ashcroft's potential gives a good fit to the transport properties in liquid gallium and to the ion-ion interactions determined from structure-factor measurements.

II. DETAILS OF CALCULATION

This calculation used the standard local-pseudopotential method without spin-orbit effects. The method will not be discussed here since it has been described in detail by Harrison[10] and by Heine.[11]

One of the problems in this particular calculation was the selection of a secular equation large enough to ensure reasonable convergence of the energy eigenvalues without using excessive computer time. Convergence tests at the center of the Brillouin zone (Γ) indicated that the eigenvalues had converged to about 0.003 Ry when 85 lattice vectors were included. To retain this degree of convergence and make the calculations more economical, the Löwdin[12] technique, as applied by Harrison and by Heine, was used to truncate the larger matrix to a smaller one. The actual procedure was to form around a particular point in k space a complete star of lattice vectors with lengths less than $Q=k/2k_F=1.26$ and construct the pseudopotential equivalent of the Hamiltonian matrix for these states. Depending on the particular point in the Brillouin zone, the dimension of this matrix varied from 85 to 100. This matrix was first reduced using the Löwdin procedure to a matrix approximately of order 30 (also containing a complete star of vectors) and then diagonalized to obtain the eigenvalues and vectors. Complete stars of wave vectors were used to preserve the symmetry-induced degeneracies. The truncation procedure introduced an additional error so that the final eigenvalues are precise to about 0.005 Ry.

A second and more fundamental problem was that of determining the appropriate pseudopotential. However, since the matrix elements of the potential v can be separated into a structure factor $S(\mathbf{k}-\mathbf{k}')$ and a form factor $V(k-k')$, i.e.,

$$\langle k|v|k'\rangle=S(\mathbf{k}-\mathbf{k}')V(k-k'),$$

the problem reduces down to determining the best form factor. The initial form factor was a "best guess" by Heine[13] based on the screened model potential calculated by Animalu and Heine[6] and the potentials used by Cohen and Bergstresser[7] in their calculations for GaP, GaAs, and GaSb. This form factor was then modified to optimize the agreement between the calculation and the experimental Fermi-surface data. The two criteria used to select the optimum form factor were: (1) that the Fermi surface allowed open-cyclotron orbits in the k_x and k_z directions, as deduced experimentally from magnetoresistance data[3,14,15]; and (2) that the cross section of the "butterfly" in the $k_z=k_c$ plane fit the rf size-effect data of Fukumoto and Strandberg.[16]

Analytic expressions for the two best form factors are

$$V5=0.604(Q-0.82)(1.52-Q)\times[1+0.15(1.17-Q)],\quad Q\leq 1.52$$
$$V5=0,\quad Q>1.52$$

and

$$V12=0.72(Q-0.85)(1.5-Q)\times[1+0.1(1.15-Q)],\quad Q\leq 1.5$$
$$V12=0,\quad Q>1.5$$

where $Q=k/2k_F$. These two form factors, plus the form factors for Inglesfield's[8] best potential (V_I6) and for the Cohen-Bergstresser[7] potentials, are shown in Fig. 1. The form factor for the Animalu-Heine[6] model potential is identical to V_I6 up to $Q=0.8$, where it then rises to a value of $V=0.096$ Ry at $Q=1.1$ instead of $V=0.08$ Ry at $Q=1.15$, as for V_I6. The form factor for the model potential calculated by Ashcroft[9] lies to the left of the curves in Fig. 1 for $Q<0.78$, has its first zero at $Q=0.78$, and has a first maximum of $V=0.095$ Ry at $Q=1.2$. From testing a variety of form factors it is evident that the better form factors have a first zero at $Q=0.81$–0.85 and a first maximum of $V\approx 0.08$ Ry at $Q=1.15$–1.2. These produced Fermi surfaces which had basically the correct shape and were approximately correct in size. However, the connectivity of the surface

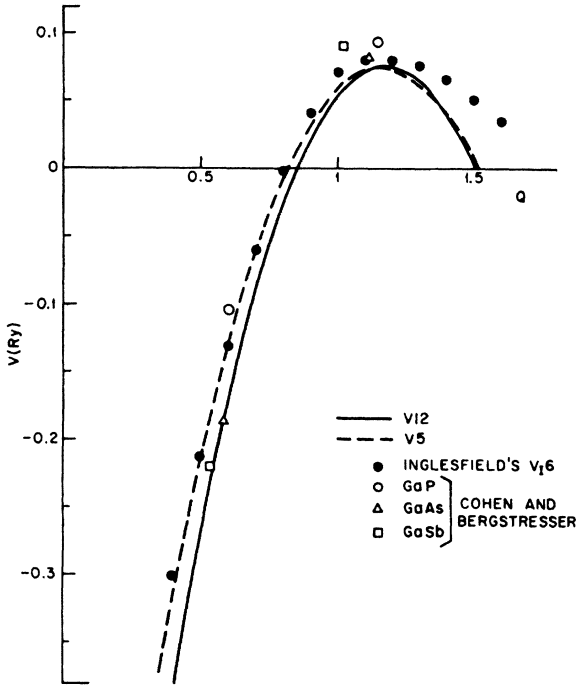

FIG. 1. Pseudopotential form factors for gallium.

[10] W. A. Harrison, *Pseudopotentials in the Theory of Metals* (W. A. Benjamin, Inc., New York, 1966).
[11] V. Heine, in *The Physics of Metals: I. Electrons*, edited by J. M. Ziman (Cambridge University Press, New York, 1968).
[12] P. O. Löwdin, J. Chem. Phys. 19, 1396 (1951).
[13] V. Heine (private communication).
[14] J. R. Cook and W. R. Datars, Ref. 2.
[15] J. C. Kimball and R. W. Stark, Ref. 2.
[16] A. Fukomoto and M. W. P. Strandberg, Ref. 2.

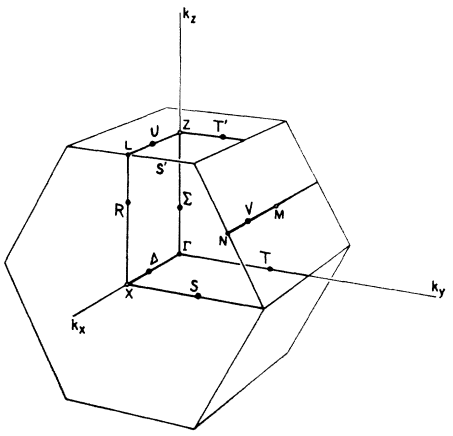

FIG. 2. Brillouin zone for gallium.

along the k_a direction was very sensitive to the exact details of the form factor.

Inglesfield[17] has tested both $V5$ and $V12$ to see if they predict the correct phase changes in the crystal structure. He finds that $V5$ predicts the phase changes correctly (but not as well as V_I6), whereas $V12$ predicts that no phase changes will occur. Unfortunately, the crystal-structure and Fermi-surface criteria are not self-consistent since $V12$ satisfies the Fermi-surface conditions better.[18] This may be due to the fact that both calculations used local pseudopotentials and a nonlocal potential is really required. Although $V5$ is a better compromise between the structure and Fermi-surface criteria, $V12$ was used since the goal of this calculation is to interpret the experimental Fermi-surface data.

The crystal structure of gallium is base-centered orthorhombic (D_{2h}) with eight atoms per unit cell. The lattice constants at 4.2°K are[19] $a=4.5103$ Å, $b=4.4861$ Å, and $c=7.6463$ Å. The primitive cell, however, contains only four atoms located at $(m,0,p)$, $(\bar{m},0,\bar{p})$, $(m+\frac{1}{2}, 0, \bar{p}+\frac{1}{2})$, and $(\bar{m}+\frac{1}{2}, 0, p+\frac{1}{2})$, where[20] $m=0.0785$ and $p=0.1525$. These lattice constants differ by about 0.1% from those used by Wood,[5] but changing from one set of constants to the other changes the energy eigenvalues by approximately 0.002 Ry, which is inside the estimated error of this calculation. The Brillouin zone for gallium is shown in Fig. 2. The notation for the symmetry points is the same used by Slater *et al.*[4]

The energy bands were computed at 115 points in the $\frac{1}{8}$ Brillouin zone on the same mesh used by Wood,[5] and the symmetry of the states determined from the character tables of Ref. 4. The Fermi energy, calculated by assuming an average of six full bands and counting states, was found to be $E_F=0.713$ Ry on an arbitrary energy scale where $\Gamma_1^+=-0.064$ Ry. The total width of the occupied bands is 0.777 Ry, which is essentially equal to the free-electron value of 0.774 Ry.

The cross sections of the Fermi surface were determined in several planes perpendicular to k_x, k_y, and k_z. The spacings of the planes were $\frac{1}{16}k_a$, $\frac{1}{16}k_b$, and $\frac{1}{8}k_c$, respectively. The Fermi-surface contours were found by searching for the change in sign of the determinant of the secular equation.

III. RESULTS OF CALCULATION

The energy bands along the various symmetry directions are shown in Fig. 3 and a perspective drawing of

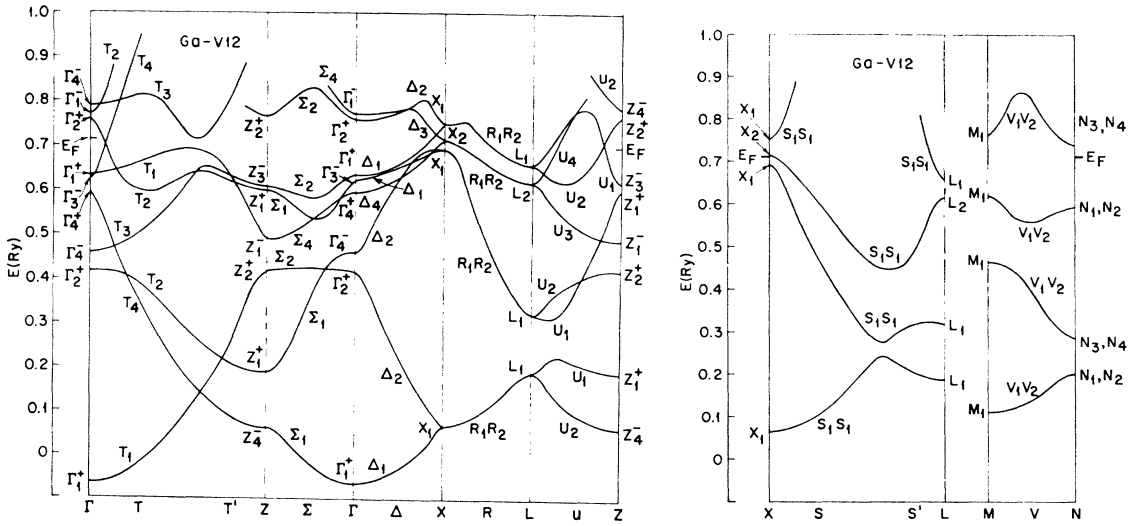

FIG. 3. Energy bands for gallium along major symmetry lines.

[17] Private communication. I am indebted to J. E. Inglesfield for testing these two potentials.
[18] Although the potentials were compared initially over only a small part of the Fermi surface, $V12$ was compared to $V5$ over all critical portions of the surface and found to be slightly better.
[19] C. S. Barrett, as quoted in Ref. 3.
[20] A. J. Bradley, Z. Krist. **91**, 302 (1935).

the Fermi surface in $\frac{1}{8}$ of the Brillouin zone is shown in Fig. 4.

Since gallium is compensated,[3] the Fermi surface should have equal volumes of holes and electrons. The equivalence of holes and electrons was checked by a crude numerical integration over the cross sections and found to be correct to about 5%.

The Fermi surface consists of an ellipsoid of eighth-band electrons centered around L, which is nested inside a "butterfly" of seventh-band electrons. These two pieces are degenerate on the $k_x=\frac{1}{2}k_a$ face, although the inclusion of spin-orbit coupling would remove this degeneracy except along the XRL line.[21] Saucer-shaped pieces of seventh-band electrons lie along the U line at $k_x\approx(3/32)k_a$ and along the T line at $k_y\approx\frac{1}{16}k_b$. A "monster" of sixth-band holes (five occupied bands) contacts the $k_x=0$ and $\frac{1}{2}k_a$ planes as well as the $k_z=0$ and k_c planes. This is a highly contorted piece, and the back side (or is it the front?) of this piece is shown in Fig. 5. At X there is also a small ellipsoid of fifth-band holes. This piece is degenerate with the 6h sheet in the $k_x=\frac{1}{2}k_a$ plane, but as before, this degeneracy will be lifted with the inclusion of spin-orbit coupling except along XRL.

In Fig. 4 there is also shown a small pancake of sixth-band holes located at $k_y\approx(17/32)k_b$ along the T line and a small ellipsoid of eighth-band electrons nested inside a crossed-disk piece of seventh-band electrons located at N. These two pieces were constructed by shifting the Fermi energy by the amounts indicated in Fig. 4. The shifting of the Fermi energy in various parts of the zone is somewhat analogous to using a nonlocal potential and will be rationalized later in the paper by appealing to the experimental data.

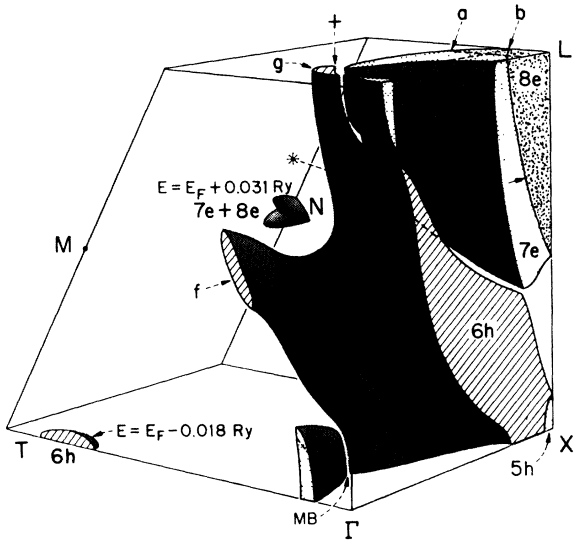

FIG. 4. Fermi surface for gallium (in $\frac{1}{8}$ of Brillouin zone); 5h and 6h indicate fifth- and sixth-band hole surfaces, 7e and 8e indicate seventh- and eighth-band electron surfaces.

IV. COMPARISON OF RESULTS TO EXPERIMENTAL DATA

A large amount of data relating to the Fermi surface of gallium has been taken using a variety of experimental techniques.[2] Much of the data is redundant, and in some cases, inconsistent. Therefore, this calculation is specifically compared to only those data which are most complete and presumably self-consistent.

A. de Haas–van Alphen Data

A comparison between the measured de Haas–van Alphen frequencies and those calculated from the present model is contained in Table I. The entries in the columns marked T contain the calculated frequencies, while the columns marked E contain the measured frequencies taken from the data of Goldstein and Foner (GF)[22] and of Condon.[23] The Arabic letters refer to the orbits indicated in Figs. 4–6; the Greek letters refer to the data of Condon (see Appendix); the Roman numerals refer to the data of GF. Breakdown indicates that the orbit is constructed assuming magnetic breakdown, and GF indicates a frequency reported by Goldstein and Foner but not labeled. The areas of the model used to calculate the frequencies were measured with a planimeter. The estimated error is about 5%.

The calculated pieces along T (7e and 6h) can be matched quite well with the data. The shapes of these two pieces are precisely those required by the data, and the actual areas are in reasonable agreement. The size

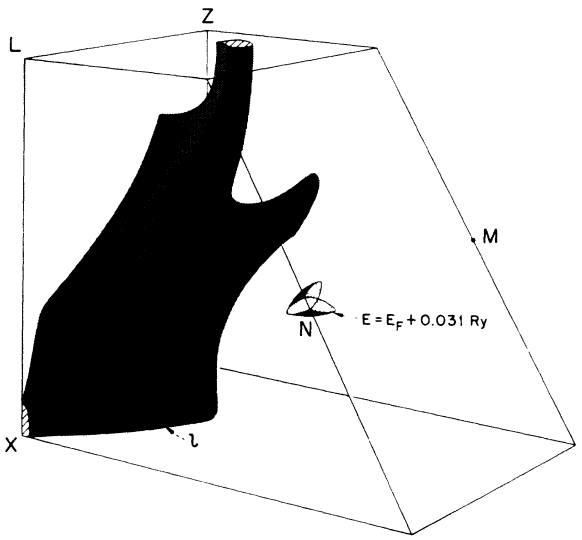

FIG. 5. Fermi surface for gallium (in $\frac{1}{8}$ Brillouin zone): Multiply connected surface is sixth-band hole; nested surfaces at N are seventh- and eighth-band electrons.

[21] G. F. Koster, Phys. Rev. **127**, 2044 (1962). The twofold degeneracy which exists at any point on the hexagonal face and at all points along MVN is removed by spin-orbit coupling *except* along the line XRL and at point M.

[22] A. Goldstein and S. Foner, Ref. 2.

[23] J. H. Condon, Ref. 2.

TABLE I. de Haas–van Alphen comparison.

Piece	Frequencies (in 10^6G) $H\|\|a$		$H\|\|b$		$H\|\|c$	
	T	E	T	E	T	E
8e ellipsoid (L)	12.2	14.3 α'	20.9 d'	19.0 α', GF	3.94	
7e butterfly (L) (central orbits)	12.2	14.3 α'	35.9 d		21.8	20.5 XV
7e butterfly (L) (noncentral orbit)	22.2 a	23.0 α, X	42.6 b	43.3 ξ		
7e butterfly (L) (noncentral) breakdown ($\frac{1}{2}$7e+$\frac{1}{2}$8e)			21.5 b	22.5 GF		
7e butterfly (L) (central) breakdown ($\frac{1}{2}$7e+$\frac{1}{2}$8e)			28.4 d, d'	30 α, X	12.7 c	12.8 α, XI
7e saucer (on T)	0.704	0.87 β, V	6.65	7.15 β	0.843	0.765 VI
7e saucer (on U)	5	···	0.705	0.725 VIII	0.468	0.425 GF
6h monster	0.458 to 1.0 f	0.77 ϵ	52(26.4) i (i, breakdown)	···	0.37 g	···
6h monster	0.37 k	···			11.2 j	
6h monster					21.8]	
6h monster (breakdown to 5h at X)					10.9]	8.5 XIII, XVIII
6h on T	0.52	0.5 γ, IV	0.346	0.342 γ, I	1.26	1.35 γ
7e at N	0.22	0.25 η	0.42		0.55	
8e at N	0.22	0.25 η	0.14		0.26	

	$H\|\|[011]$		$H\|\|[0\bar{1}1]$	
	T	E	T	E
7e at N	0.52		0.65	
8e at N	0.11		0.47	

of the 6h piece is of course arbitrary since E_F was adjusted at this point in the Brillouin zone to create it. However, the energy was picked by *only* matching the k_z dimension to the data and letting the other dimensions come out of the calculation for that energy. The important point to note is that having fixed one dimension to experiment, the correct anisotropy is then determined. From Condon's data we calculate the ratios of the areas to be $a:b:c=1.46:1:3.95$, and from the model we calculate $a:b:c=1.5:1:3.66$. This good agreement with the data is considered sufficient reason for shifting the Fermi energy at this point.

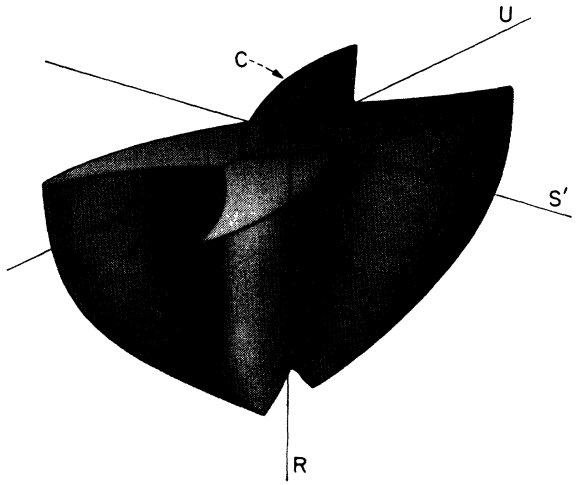

FIG. 6. Butterfly complex of seventh- and eighth-band electrons located at L. Two-winged orbit caused by magnetic breakdown labeled C.

The 7e and 8e surfaces centered at L can also be matched with the data. The frequencies X, XI, and XVI reported by GF and the α branches reported by Condon are associated with these pieces, but are misleading since not all parts of these branches are associated with central orbits. The data can be most easily explained by referring to Condon's data (see Appendix). For the field along the a axis the model has an extremum at $k_x=\frac{1}{2}k_a$ (the hexagonal face). This is a maximum for the 8e piece and a minimum for the 7e piece and corresponds to a frequency of 12.2 MG. The maximum for the 7e piece lies in the plane $k_x\approx\frac{3}{8}k_a$ (Fig. 4, orbit a) and has a corresponding frequency of 22.2 MG. Referring to Condon's data, we see that for $H\|a$ there is a frequency 14.3 MG (α') which splits as the field is rotated away from the axis. This then is associated with the central orbits. The α frequency for $H\|a$ is 23.0 MG and corresponds to the noncentral maximum of the model. For $H\|b$ the central orbits have frequencies of 20.9 MG (8e, orbit d') and 35.9 MG (7e,

orbit d) and a magnetic breakdown orbit composed of $\frac{1}{2}$ of an $8e$ orbit and $\frac{1}{2}$ of a $7e$ orbit (d plus d') with a frequency of 28.4 MG. In addition there is a noncentral maximum on $7e$ at $k_y \approx \frac{1}{16} k_b$ (orbit b) with the possibility of magnetic breakdown onto the $8e$ piece. The frequencies for these noncentral orbits are 42.6 and 21.5 MG, respectively. Again referring to the data, we matched the 19.0-MG (α') and 30-MG (α) frequencies with the $8e$ central orbits and $\frac{1}{2}8e+\frac{1}{2}7e$ breakdown orbits. The 43.3- and 22.5-MG (GF) frequencies we then match with the noncentral orbit without and with breakdown. The fact that Condon only sees the 43.3-MG frequency (no magnetic breakdown) and GF only see the 22.5-MG frequency (with magnetic breakdown) strengthens this assignment since Condon's maximum field was 32 kOe, whereas GF worked at 60 kOe. For $H \| c$ the model has a four-winged butterfly orbit on $7e$ (21.8 MG), an elliptical orbit on $8e$ (3.94 MG), and a two-winged butterfly (orbit c in Fig. 6) due to breakdown between $8e$ and $7e$ (12.7 MG). Experimentally there are no frequencies which can be matched to $8e$, but the 20.5-MG (GF-XV) and 12.8-MG (α) frequencies can be matched with the four-winged and two-winged butterflies, respectively.

For all of its complexity, the large $6h$ band-hole monster has relatively few extremal areas for the field along the principal axes. For $H \| a$, the only extrema are at $k_x=0$ and $\frac{1}{2}k_a$. The size of the arm at $k_x=0$ is very sensitive to E_F; a decrease of 0.003 Ry in E_F doubles the area, whereas it disappears completely with an increase of 0.002 Ry. The frequency associated with this piece is 0.45 MG (orbit f) and it is tentatively matched with frequency ϵ in the data. The neck at $k_x=\frac{1}{2}k_a(X)$ is probably much too large. If the extremely small closed sheet (δ) seen by Condon is associated with the fifth band-hole ellipsoid located at X, then the $6h$ neck must shrink. This is because these two surfaces are degenerate along XRL, even with the inclusion of spin-orbit coupling. Assuming the surface responsible for the δ frequencies is an ellipsoid, the calculated radius along k_z (and thus the linear dimension of the $6h$ piece from X along XRL) is 0.0046 a.u.$^{-1}$. This is an order of magnitude smaller than the 0.037 a.u.$^{-1}$ measured on the model. The only other orbit on the $6h$ monster that can be matched with the de Haas–van Alphen data is labeled l in Fig. 5. This is a two-winged orbit which results from magnetic breakdown and has a frequency of 10.9 MG. This is matched to the 8.5-MG (XIII) frequency which GF claim is involved in breakdown. The relationship between frequencies XIII, XI, and XV, which GF comment on, is considered to be fortuitous.

The matching of the frequencies for the $7e$ piece located along U to the experimental data is somewhat tenuous. Although the frequencies listed in Table I are in close agreement and have the right angular dependence, the angular extent of the data is too limited to make the assignment certain.

After removing all frequencies which can be matched to the model, a considerable number of frequencies, especially small ones, remain unassigned. The intermediate and high frequencies might be dismissed by stating that they are due to the $6h$ monster, even though the exact assignment cannot be made. However, the low frequencies cannot be accounted for in this manner since a sufficient number of small areas could not possibly exist on this piece. Assuming that other small pieces must exist, the Fermi energy was raised and lowered in search of new pieces. Lowering the energy to $E=E_F-0.018$ Ry produced no new surfaces other than the $6h$ holes on T which have already been discussed. Raising the energy produces an almost spherical piece located at $k_y \approx \frac{5}{8} k_b$ for $E \geq E_F+0.002$ Ry, but it was rejected because it is located where the energy was reduced to produce the $6h$ surface. The next piece of new surface is at N for $E=E_F+0.031$ Ry. This energy was picked so that the area of the surface for $H \| a$ was equal to the frequency η seen by Condon. The experimental frequency splits into two branches as the field rotates away from the a axis, which is the behavior expected for this nested surface. Frequencies calculated from the model are listed in the table, but no assignments are made.

B. rf Size-Effect Data

The most complete rf size-effect data on gallium have been reported by Fukumoto and Strandberg[16] (FS) and by Haberland, Cochran, and Shiffman[24] (HCS). In general, both sets of data agree where they overlap; FS concentrating on the large dimensions and HCS concentrating on the smaller dimensions. Table II summarizes the identification of the data to the model. The subscripted letters refer to HCS and the numbers refer to FS.

The most complete data are for the electron pieces at L which are associated with data labeled 12, 13, C_4, C_5, and C_6. Figure 7 compares the data with the model in the ab and bc planes. The solid lines represent both the data and the model, the dotted lines are for the model, the dashed lines are the data of HCS, and the dashed-dot lines are the data of FS. The agreement is quite good except at the tip of the wings, where nobody seems to agree. The C_5 lines are the result of the noncentral extremal orbits discussed in Sec. IV A. The planes in

TABLE II. rf size-effect identification.

Piece	bc plane	ac plane	ab plane
$8e$ at L			C_6, 13
$7e$ at L	A_4, 1	5, 6	C_4, C_5, 12
$7e$ on T	A_3		C_7[a]
$6h$ on T	A_2	B_2[b]	
$6h$ monster		7	11
$7e$ at N	$A_1(?)$		$C_1(?)$
$8e$ at N		$B_3(?)$[c]	$C_2(?)$

[a] C_7 is the unlabeled branch in Fig. 5(c) of HCS.
[b] B_2 is the unlabeled branch which contacts the k_c axis in Fig. 5(a) of HCS.
[c] B_3 is the unlabeled branch that contacts the k_a axis in Fig. 5(a) of HCS

[24] P. H. Haberland *et al.*, Ref. 2.

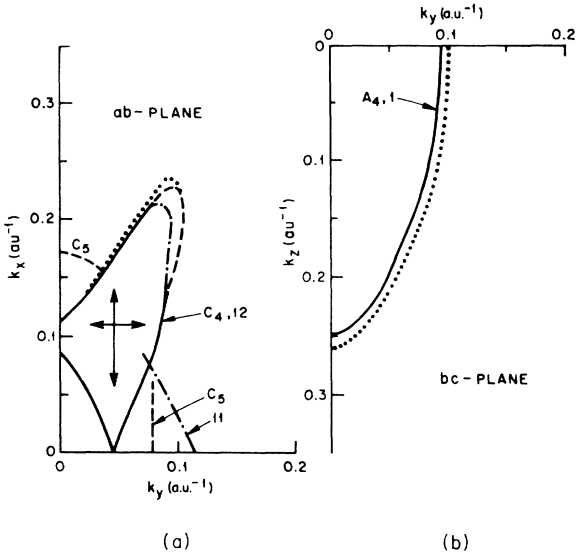

FIG. 7. Comparison of rf size-effect data with model. Dotted lines are calculated from model, dashed lines are from HCS and dash-dot lines are from FS. Solid lines are where model, HCS, and FS all agree. In (a), the horizontal and vertical arrows indicate planes of noncentral extremal orbits that occur when the field is parallel to the k_x and k_y axes.

which these orbits occur for the field along the k_x and k_y axes are indicated by the vertical and horizontal arrows. In the *bc* plane, the data and the model agree well in shape although the model predicts consistently larger k vectors. Branches 5 and 6 of FS taken in the *ac* plane are associated with orbits around the wings of the butterfly. The dimensions agree with the model about as well as the data and model agree in Fig. 7(b).

The *7e* piece on T can be matched with the A_3 and C_7 branches of HCS. Over the angular range on which the data were taken, these branches are not expected to show a closed piece. There is, however, one point which makes this identification convincing. The data indicate for $H \perp b$ that the k_y dimension is 0.007 a.u.$^{-1}$ in the A crystal and 0.011 a.u.$^{-1}$ in the C crystal. The model predicts just such a difference with $k_y=0.008$ and 0.012 a.u.$^{-1}$ for the two cases. This difference in k_y for the two field directions is a result of the piece being saucer-shaped in the $k_x=0$ plane and ellipsoidal in the $k_z=0$ plane.

The A_2 branch reported by HCS matches very well with the *6h* piece located on T. It shows a closed flat ellipsoid with radii along the axes of $k_z=0.011$ and $k_y=0.038$ a.u.$^{-1}$. This agrees with $k_z=0.011$ and $k_y=0.041$ a.u.$^{-1}$ measured on the model. The B_2 branch has the correct k_z dimension, but is not followed over a large enough angular range to make the identification positive. It would have to contact the k_x axis at 0.026 a.u.$^{-1}$ for it to agree with the model.

On the *6h* monster a good match can be made with the 7 and 11 branches of FS. The orbit for branch 7 is labeled 7 in Fig. 4 and the orbit for 11 ($H \| a$) is shown in Fig. 5. Other branches such as 3, 10, and the unlabeled A branch in Fig. 6 of HCS can also be placed on *6h*. However these assignments are very questionable, since the surface is sufficiently convoluted and the branches are observed over a small enough angular range as to make the identification tenuous.

As was the case in the de Haas–van Alphen data, a number of small k vectors measured by the rf size effect indicate additional small pieces of Fermi surface. *Very* tentative assignments have been made for A_1, B_3, and C_1 on the crossed-disk surface at N, but there still remains a reasonable amount of data unexplained.

C. Magnetoacoustic Data

The magnetoacoustic data for the *ab* plane reported by Lewiner[25] contains essentially the same data reported by Fukumoto and Strandberg.[16] The curves labeled I, II, and III by Lewiner correspond to curves 13, 12, and 11 of FS. The only difference in the data is for **k** vectors near the k_x axis on curve II (12). Lewiner reports a bump on the wing of the butterfly which is seen neither by FS nor by HCS. Since no extremum with this dimension has been found at this angle on the model, the source of these data is unknown.

Additional magnetoacoustic data have been reported by Bezuglyi, Galkin, and Zhevago[26,27] (BGZ). They report a closed surface in the *bc* plane (Fig. 6 of Ref. 8), which is a slightly bulged ellipsoid with radii along the axes of $k_y=0.022$ and $k_z=0.012$ a.u.$^{-1}$. Although the general shape is correct, this closed sheet cannot be matched with the *6h* piece on T since the k_y dimension differs by a factor of 2. In the *ac* plane (Fig. 3 of Ref. 27) they report what appears to be a surface open along k_c. However, over the range of angles in which these data were followed, the **k** vectors match well with the *7e* piece located on U. BGZ measure $k_x=0.006$, compared to 0.007 a.u.$^{-1}$ on the model, and for a **k** vector 25° from k_z they measure $k=0.016$ compared to $k=0.018$ a.u.$^{-1}$. The reason that the data do not appear to be due to an ellipsoid is that this piece is saucer-shaped in the $k_y=0$ plane.

D. Galvanomagnetic Data

From galvanomagnetic measurements on gallium, Reed and Marcus[3] concluded that the number of electrons equals the number of holes and the Fermi-surface-supported open orbits in the k_z direction for all field direction in the *ab* plane. Cook and Datars,[14] using an induced torque technique, confirm the results of Reed and Marcus and find in addition that the k_z-direction open orbits disappear for the field precisely along the *a* axis and k_x-directed open orbits exist for the field in the range 27.5°–36.5° from the *b* axis in the *bc* plane. These more recent results were simultaneously obtained by Kimball and Stark[15] (KS) using the conventional galvanomagnetic four-probe dc technique. They also report k_x-directed open orbits caused by magnetic breakdown for additional field directions in the *bc* plane.

[25] J. Lewiner, Ref. 2.
[26] P. A. Bezuglyi *et al.*, Zh. Eksperim. i Teor. Fiz., in Ref. 2.
[27] P. A. Bezuglyi *et al.*, Fiz. Tverd. Tela, in Ref. 2.

As the field is rotated an angle θ away from the b axis in the bc plane KS observed k_x-directed open orbits at (1) $\theta=17°$–$20°$ due to magnetic breakdown; (2) $\theta=28°$–$39°$; (3) $\theta=44°$–$50°$, due to magnetic breakdown with a sharp cutoff at 44° but not at 50°; (4) $\theta=60°$–$90°$ due to magnetic breakdown. In addition, in regions 3 and 4 they see large amplitude de Haas–Schubnikov oscillations which confirm the breakdown hypothesis. The approximate frequencies of these oscillations are 0.78 and 8 MG for $\theta=90°$ ($\mathbf{H}\|c$), and 0.36 MG for $\theta\approx 50°$.

The galvanomagnetic data provide the most convincing evidence that the shape of the $6h$ monster is basically correct. From Figs. 4 and 5 it is easily seen that the $6h$ surface supports open orbits along k_z for all field directions in the ab plane. However, close inspection reveals that for $H\|a$ these orbits disappear since the point in the $k_z=k_c$ plane labeled with a cross (+) in Fig. 4 lies closer to the $k_x=0$ plane than the point labeled with an asterisk (*). This then agrees with the experimental observation that no k_x-directed open orbits exist for H exactly parallel to the a axis. At high fields, these open orbits might appear as a result of magnetic breakdown between the $6h$ piece and either the $7e$ ellipsoid on U or the $7e$ butterfly.

The model also explains the data for H in the bc plane. The arm (f) in the $k_x=0$ plane and the small neck at X allow k_x-directed open orbits for H in a range $\theta=28°$–$34°$. This is slightly smaller than the measured range, but decreasing E_F by only 0.003 Ry is sufficient to obtain agreement.

For $H\|c$ the k_x-direction open orbits due to magnetic breakdown are in the $k_z=0$ plane and run along the $7e$ piece on T, across the gap at the point labeled MB in Fig. 4, and continue on the $6h$ monster and into the next zone at X. This orbit is verified by the frequency of the oscillations. The 0.78-MG frequency agrees with the de Haas–van Alphen frequency assigned to the $7e$ piece and the 8-MG frequency agrees with the de Haas–van Alphen frequency assigned to the $6h$ piece (orbit 1 in Fig. 5). Since the latter frequency is itself due to breakdown between the $5h$ and $6h$ piece, these open orbits should disappear again at higher fields. Since the energy gap between the $7e$ and $6h$ pieces is small over a large part of $7e$, the angular range of this type of breakdown orbit will extend away from the c axis until there no longer exists a plane perpendicular to the field which contains the small neck at X and the $7e$ ellipsoid.[28] The angle at which this happens on the model is $\theta=45°$. The cutoff should be sharp since these orbits are no longer topologically possible. The $\theta=45°$ limit agrees with the 44° sharp cutoff of region 2 in the data. It therefore seems reasonable that regions 2 and 3 are the same, but for $\theta=50°$–$60°$ the gap increases so that no breakdown occurs at the fields used.

For $\theta\approx 50°$ the oscillations reported by KS must still be due to the $7e$ piece along T. However, the orbits which lie in a plane that must also contain X are the nonextremal orbits labeled p in Fig. 4. Although the frequencies measured are usually due to extremal orbits, it seems possible that the frequency of nonextremal orbits might be measured when coupled with magnetic breakdown. An estimate of the frequency of these orbits on the model is 0.45 MG. Since small changes in the exact size and shape of the $7e$ piece would change this frequency considerably, the agreement is good with the measured frequency of 0.36 MG. If the interpretation is valid, this is probably the first experimental verification of magnetic breakdown causing oscillations from nonextremal orbits.

After studying the model Fermi surface one concludes that the magnetic breakdown observed in region 1 probably does not create open orbits, but causes a loss of compensation. KS conclude that there are open orbits along k_a, but only discuss the data for $J\|b$, and do not discuss the data for $J\|a$. A magnetoresistance that saturates at high fields after an initial quadratic dependence would also occur if the metal became uncompensated due to breakdown. On the model, region 1 is the range of angles which allow orbits to run along the arm of the $6h$ monster, across the gap onto the $7e$ surface on T, and across the gap again and back onto the $6h$ arm. This large orbit would be electronlike and therefore break the compensation.

E. Resistivity Anisotropy

The dc resistivity of gallium is highly anisotropic, the ratios of the resistivities[29] at 77°K being $\rho_a:\rho_b:\rho_c=2.14:1:7.43$. This indicates that Fermi velocities are largest in the y direction and smallest in the z direction or, in different terms, that the radius of curvature[24] of the surface is largest in the y direction and smallest in the z direction. As can be seen in Figs. 4 and 5, the model exhibits these properties and is in qualitative agreement with the data.

V. RELATION OF ELECTRONIC STRUCTURE TO CRYSTAL STRUCTURE

Heine[30] has studied the crystal structure of gallium and finds, although it is too complex to derive theoretically, that it "makes sense" with regard to the number of nearest neighbors, their distances, and covalency. He notes that the large number of zone planes which just cut the free-electron sphere should cause an energy gap at the Fermi level throughout most of the Brillouin zone. This has the effect of eliminating a large fraction of the 1-OPW Fermi surface, especially in the k_z direction, and is the source of the anisotropy in the resistivity discussed in Sec. IV. Heine suggested that the gap is in some sense a measure of the covalency.

The present calculation supports quite well the work of Heine. When the energy bands in Fig. 3 are compared to the free-electron bands,[4] it can be seen that a gap of $\sim$0.1 Ry has appeared at the Fermi level around Γ, Z,

[28] I have assumed that the neck at X has shrunk to make it compatible with the assignment of Condon's δ frequency to the $5h$ surface at X, as discussed earlier.

[29] W. A. Reed and J. A. Marcus, Phys. Rev. **130**, 957 (1963).

[30] V. Heine, J. Phys. **C1**, 222 (1968).

and M and along most of Σ, Δ, T, and T'. This suggests that there is a certain amount of covalency in gallium.[31]

VI. SUMMARY

After comparing the results of this calculation with the experimental data, it is concluded that the model represents reasonably well the Fermi surface of gallium. However, the data also indicate that in addition to the pieces described here, there probably exists one or more small pieces with dimensions $\leqq 0.01$ a.u.$^{-1}$. Hopefully this calculation will encourage a further refinement of the experimental data, which in turn will lead to more sophisticated calculations.

ACKNOWLEDGMENTS

I am deeply indebted to V. Heine for suggesting this problem and for help in its early stages. Likewise, I am indebted to L. F. Mattheiss for his many suggestions and encouragement and for critically reading the manuscript. I wish to thank J. H. Condon not only for many helpful discussions, but also for allowing me to publish his de Haas–van Alphen data in the Appendix. I also want to thank C. H. Shiffman, R. Datars, and R. W. Stark for copies of their data prior to publication. Finally, I am indebted to R. A. Faulkner for supplying me with copies of his very efficient matrix diagonalization and determinant programs.

APPENDIX

Figure 8 is a reproduction of the de Haas–van Alphen data taken by Condon[23] in magnetic fields up to 33 kOe by the torsion method. Figure 9 shows the Fermi surfaces constructed by Condon from the four closed periods labeled α, β, γ, and δ in Fig. 8.

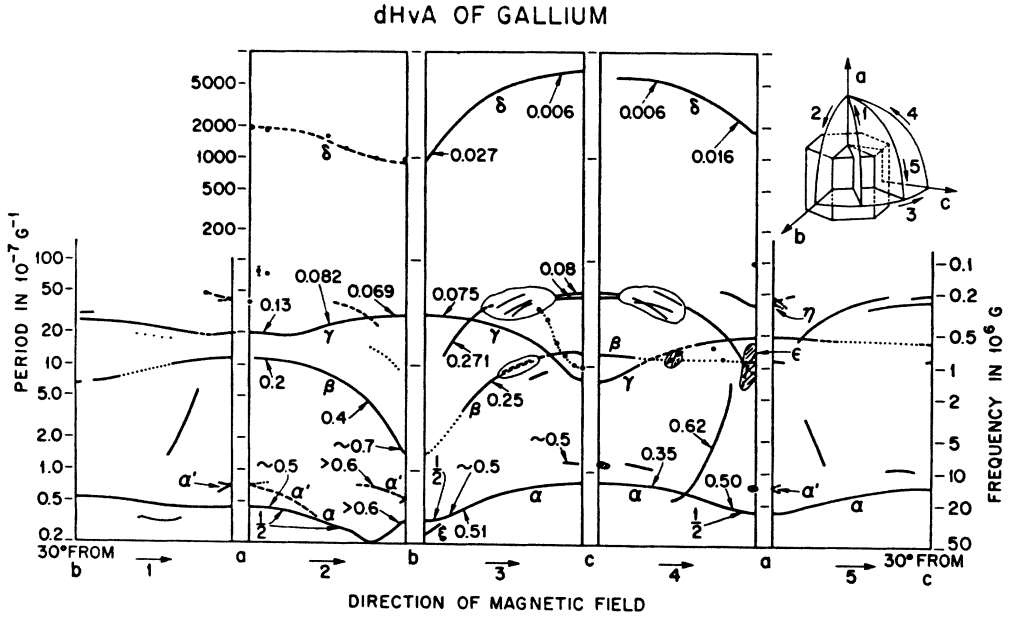

FIG. 8. de Haas–van Alphen data for gallium taken by Condon.

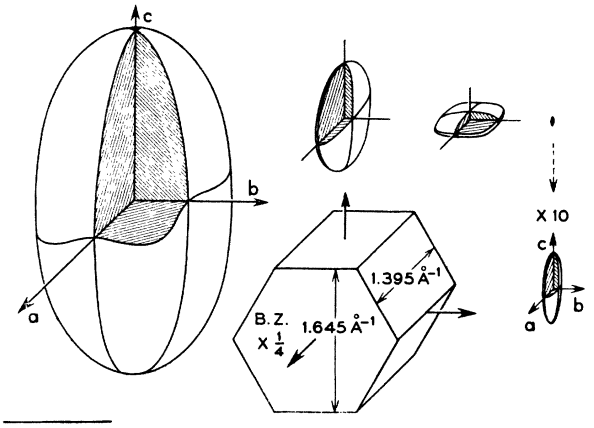

FIG. 9. Fermi-surface pieces as constructed by Condon from data in Fig. 8. In descending size, pieces represent branches α, β, γ, and δ, respectively.

[31] I want to thank J. C. Phillips for bringing this point to my attention.

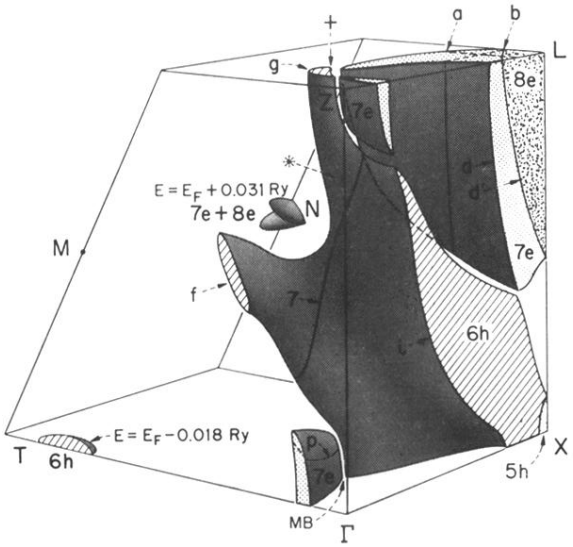

FIG. 4. Fermi surface for gallium (in $\frac{1}{8}$ of Brillouin zone); 5*h* and 6*h* indicate fifth- and sixth-band hole surfaces, 7*e* and 8*e* indicate seventh- and eighth-band electron surfaces.

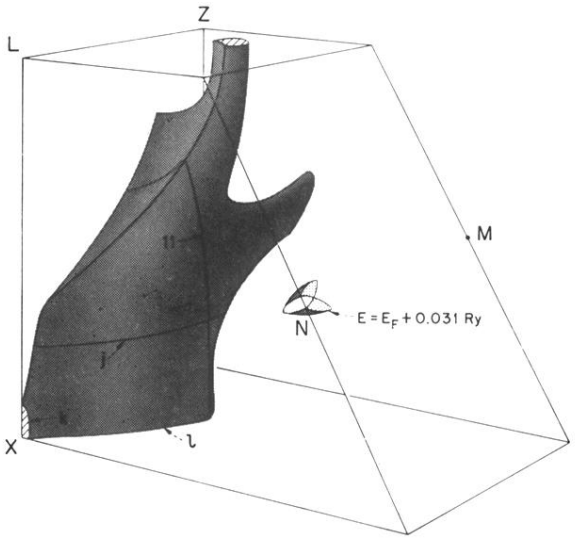

FIG. 5. Fermi surface for gallium (in $\frac{1}{8}$ Brillouin zone): Multiply connected surface is sixth-band hole; nested surfaces at N are seventh- and eighth-band electrons.

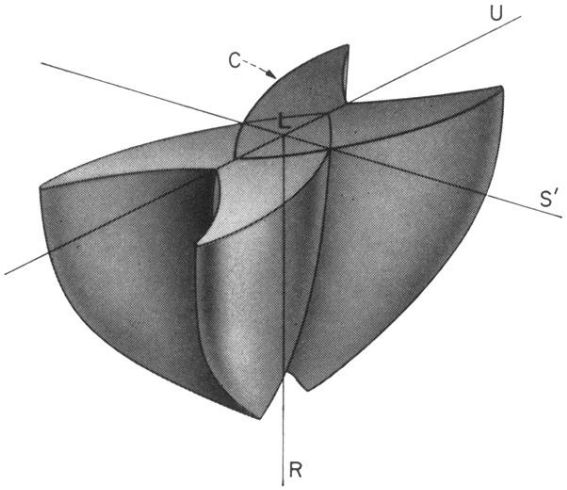

FIG. 6. Butterfly complex of seventh- and eighth-band electrons located at *L*. Two-winged orbit caused by magnetic breakdown labeled *C*.